NANO-MICRO LETTERS ARTICLE
www.nmletters.org

Using Inductance as a Tuning Parameter for RF Meta-atoms

Derrick Langley[1*], Ronald A. Coutu, Jr.[2*], Peter J. Collins[2]

(Received 2 March 2012; accepted 30 June 2012; published online 28 June 2012.)

Abstract: The resonant frequency of metamaterials structured with split ring resonator (SRR) meta-atoms is determined primarily through the capacitance and inductance of the individual meta-atoms. Two designs that vary inductance incrementally were modeled, simulated, fabricated, and tested to investigate the role inductance plays in metamaterial designs. The designs consisted of strategically adding sections to the SRR to increase the inductance, but in a manner that minimized capacitance variations. Each design showed a shift in resonant frequency that was proportional to the length of the added section. As the length of each section was increased, the resonant frequency shifted from 2.78 GHz to 2.18 GHz.
Keywords: Inductance; Meta-atom; Metamaterial; Split Ring Resonator; Radio Frequency; Resonance

Citation: Derrick Langley, Ronald A. Coutu, Jr. and Peter J. Collins, "Using Inductance as a Tuning Parameter for RF Meta-atoms", Nano-Micro Lett. 4 (2), 103-109 (2012). http://dx.doi.org/10.3786/nml.v4i2.p103-109

Introduction

Metamaterials are engineered materials commonly fabricated from metal structures deposited on electrically isolated dielectric substrates. These materials, according to Pendry [1], can result in unique material properties that do not exist in nature such as negative permeability (μ) or negative permittivity (ε), and therefore lead to negative index of refraction (n). Smith *et al.* [2] demonstrated the first such material based on Pendry's initial work.

The split ring resonator (SRR) is commonly used as the meta-atom in the structured layer. The SRR is a commonly used component in metamaterial research ranging from radio frequency (RF) to terahertz (THz) [3-5]. The metamaterial design arranges periodic rings as elements to create an electromagnetic response to an incident electromagnetic (EM) wave at a specific frequency, from which the effective μ and ε parameters for the rings are generated [2,6]. The dimensions of the SRR, typically 10% of the incident wavelength, determine the specific resonance of the meta-atoms and the overall metamaterial. The resonant frequency (ω_{res}) is determined from the capacitance (C) and inductance (L) of the meta-atom based on the SRR structural dimensions and metal structure. For comparison, capacitance depends on the overlap area and dielectric materials between metal surfaces. Inductance depends on the metal dimensions with length being the main parameter for split-ring resonators along with the material permeability. When using capacitance as a shifting parameter, an advantage is the constant surface area associated with the parallel plate capacitor. A disadvantage is the high voltage required to shift the capacitance with electrostatic actuation of MEMS varactors [7]. When using inductance, an advantage we observe is the improved null depth at the resonant frequency. A disadvantage for using inductance to shift the resonant frequency is the amount of surface area that is required to vary the inductance. Varying the length of SRRs

[1]PhD Candidate, Air Force Institute of Technology, Wright-Patterson Air Force Base, OH 45433 USA.
[2]Assistant Professor, Air Force Institute of Technology, Wright-Patterson Air Force Base, OH 45433 USA.
*Corresponding author. E-mail: Derrick.Langley@afit.edu; Ronald.Coutu@afit.edu

is a novel method to shift the resonant frequency and provides an advantage to make the resonant frequency shift based on inductance. Many research efforts focus on the SRR to create metamaterials for applications at RF. Marques *et al.* provides ideas on various metamaterial designs [8]. Gil *et al.* demonstrated metamaterial transmission lines using subwavelength resonators imbedded in metamaterial transmission lines described in [9].

The Baseline SRR design is static with a fixed resonant frequency; therefore tunable methods are required to broaden the functions of metamaterial. Most research has focused on the changing capacitance for tuning purposes [10]. Tunable designs have successfully shown that altering the capacitance with varactors [11,12] or adding additional splits in the resonator [13] can shift the resonance in a smooth fashion. Also, incorporating microelectromechanical systems (MEMS) cantilever arrays has been shown to create frequency tuning by varying SRR capacitance [10].

There are only a few reports on changing the inductance to shift SRR resonant frequency [14,15]. In these papers, the s-shaped designs are modified to change inductance for tunable metamaterials, dual-band switches and s-shaped antennas. In this research, three designs are modeled, simulated, fabricated, and tested to determine the effects of inductance on meta-atom designs. Our approach is to identify a design that changes inductance while minimizing capacitance changes. To accomplish this, the Baseline SRR design is modified with loops on the vertical sides. Once promising designs have been identified with this static approach, future work will explore means for adaptively modifying the structure.

Theory

The SRR consisting of symmetrical rings is the basis for our current loop design. It is a resonant LC circuit that is shown to produce effective permeability and permittivity on propagating electromagnetic waves [8]. The design is based on circular double split ring resonators designed, modeled and fabricated by Marqués *et al.* However, our design and modeling deviates from Marqués *et al.* modeling based on two different characteristics [16]. First, our design is a rectangular double split ring resonator design, not a circular design. By using the rectangular design, we are able to divide the split ring resonators into sections and calculate capacitance for each section which differs from Marqués *et al.* modeling which uses the radius of the gap between the inner and outer split ring resonators. Also, the rectangular design provides the design freedom to change the design to increase the self-induction with small deviations to the total capacitance, a novel approach to shift the resonant frequency. And second, parallel traces are added to the sides of the double split ring resonators to create a low frequency plasma that effects the relative permittivity [17]. The combination of the rings and traces create a resonant frequency based on the component dimensions and metal structure.

In this work, three designs were investigated to determine the effect of increased inductance on the SRRs resonant frequency response. The relationship the inductance has on the resonance is approximated by

$$\omega_{res} \cong \frac{1}{\sqrt{LC}} \tag{1}$$

where, L and C are the inductance and capacitance, respectively. From Equation (1), the resonant frequency shifts toward lower frequencies as the inductance increases.

For the Baseline design, the resonant frequency equation can be expressed, where the inductance is self inductance of the outer and inner split ring resonator (L_{Outer}, L_{Inner}). Capacitance is determined by the capacitance at the gaps in the split ring resonators ($C_{Section\_B}$, $C_{Section\_C}$) along with the horizontal sides of the adjacent split ring resonator which is based on the series combination of the structure. Additional capacitance is generated from the vertical sides of the split ring resonator (C_{Left_Side}, C_{Right_Side}) and capacitance due to the traces (C_{Traces}). Figure 1 shows the baseline design divided into the four sections around the split ring resonators used to determine the capacitance. Figure 1 (b) shows the series resonant LC bandstop filter circuit model tailored to represent the response of the meta-atom. This model provides a response equivalent to the meta-atoms that are experimentally tested within our RF strip-line measurement setup. Furthermore, this circuit model relates the resonant frequency analytical model (ω_{res}) which defines the resonant frequency location to our design.

$$\omega_{res} = \frac{1}{\sqrt{\left(\frac{1}{\frac{1}{L_{Outer}} + \frac{1}{L_{Inner}}}\right)(C_{Section\_B} + C_{Section\_C} + C_{Left\_Side} + C_{Right\_Side} + C_{Traces})}} \tag{2}$$

To minimize the change in capacitance, the design must reduce the amount of capacitance shift while increasing the amount of inductance. The resonant equation is based on [8] and [17], but is modified based on parameter values obtained from analytical modeling and CoventorWare® Finite Element Method (FEM) simulations. The simulation computes capacitance values on each element based on the interaction with other elements. In [17] and [18], the analytic model uses capacitance of the split ring resonator gap and capacitance between the split ring resonators. Using our model, the rectangular split ring resonator is divided into sections to calculate the capacitance values.

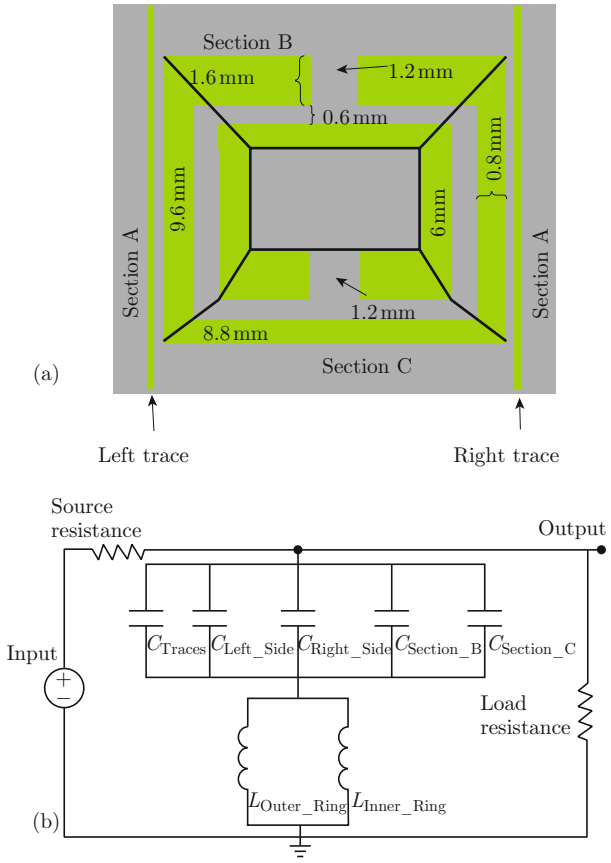

Fig. 1 (a) Baseline meta-atom indicating sections and dimensions. (b) The equivalent LC circuit model representing the meta-atom design.

The inductance depends on the type of metal, length (l), width (w), and total induced current on the component, wire, or trace. Inductance is defined as

$$L = \frac{\psi_{ij}}{I_j} \text{ for } I_k = 0 \text{ if } \; k \neq j \tag{3}$$

where ψ_{ij} represents the magnetic flux in the loop due to a current I_j in the loop j [19]. From this definition, the self-inductance of any wire, loop, or filament can be described using the dimensions of the structure and the induced current.

In [19], Ruehli provides a derivation of partial self-induction per length which leads to a simplified equation for infinitely thin conductors

$$\frac{L_{P_{ii}}}{l} = \frac{\mu}{6\pi}\Big\{3\ln[u+(u^2+1)^{\frac{1}{2}}] + u^2 + u^{-1} + 3u\ln\left[\frac{1}{u} + \left(\frac{1}{u^2}+1\right)^{\frac{1}{2}}\right] - \left[u^{\frac{4}{3}} + \left(\frac{1}{u}\right)^{\frac{2}{3}}\right]^{\frac{3}{2}}\Big\} \tag{4}$$

where μ is the permeability and u is defined as the ratio of the l to the w. For this simplified equation, the ratio of the thickness to the width of the conductor is considered less than 0.01. From this derivation, the calculation of the partial self-inductance for complex traces or circuits can be solved analytically using Equation (4). Based on this analytic equation, solvers have been developed to determine inductance of structures. CoventorWare® determines the inductance of the three designs using an integral equation approach combined with a multipole-accelerated solution algorithm [20]. Additionally, a FEM simulation is used to evaluate complex design layouts, prior to fabrication, by showing how SRR modifications affect the overall capacitance of the meta-atom structure.

Design

Figure 1 shows the Baseline design that consists of a meta-atom with inner and outer rings along with two parallel traces. The inner ring has a length of 6.0 mm for each side and a capacitive gap of 1.2 mm. The outer ring has a length of 9.6 mm for each vertical side. The outer ring's horizontal sides are 8.8 mm with a capacitive gap of 1.2 mm. The width of the rings at the capacitive gap is 1.66 mm, while the other sides of the rings have a width of 0.8 mm. The gap between the inner and outer ring is 0.6 mm. The traces adjacent to the rings are 12 mm long and have a width of 0.20 mm. The traces are spaced 0.20 mm from the outer ring. From the baseline design, structural modifications are made to increase the amount of inductance with minimal changes in the structure's capacitance.

To modify the design with minimum capacitance change, the capacitive area of each element must have minor changes. The separation gap between elements has to remain a fixed distance. To accomplish the modification, the outer ring is modified with a 0.15 mm gap in the middle of the vertical sides. Loops are added to the outer ring design which increased the overall length of the outer ring. The increased length produces a change in the inductance based on the increased path for current flow. From the baseline design, two modi-

fications are implemented with each design increasing the length of the loop which in turn increases inductance of the outer ring. Figure 2 shows the two designs used to demonstrate changes in resonant frequency as a function of the increasing length for the outer SRR.

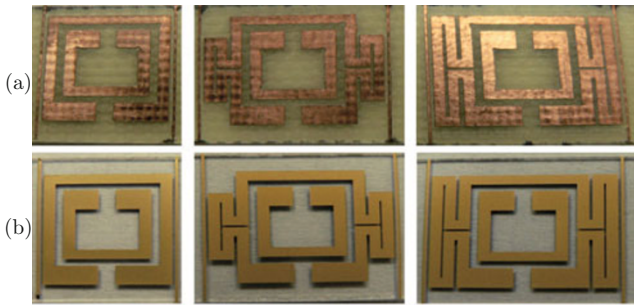

Fig. 2 Baseline, Loop A and Loop B Meta-atom designs, (a) prototypes on printed circuit board and (b) designs made by microelectronic fabrication techniques on quartz substrates.

On all the designs, the separation between adjacent meta-atom is 2.4 mm. Within the RF strip-line, the meta-atom arrays are kept apart by a 10 mm distance to form a two dimensional array above and below the center conductor. The 0.15 mm gap in the vertical sides of the outer ring is maintained on all modifications to connect the loops of the various designs. After completing the three designs, a computer simulation of each design is accomplished using CoventorWare® to determine the self-inductance and capacitance of each ring and trace.

Fabrication

Two sets of the three designs were fabricated; one set was prototyped on FR4 printed circuit board (PCB) with single sided copper and the second set was fabricated using microelectronic techniques on a quartz substrate. Figure 3 shows how the Loop B design appears when inserted into the RF strip-line. As the wave propagates down the RF strip-line, the meta-atoms affect the applied electric field (**E**) and magnetic field (**H**) when placed above and below the center conductor. In this configuration, the applied fields emulate a plane wave illumination of a larger metamaterial array.

The prototype designs, on the FR4 PCB, were completed using a T-Tech Inc. Quick Circuit 5000 milling system. From the PCB prototype devices, the fabrication transitioned to microelectronic fabrication where the meta-atoms were fabricated on semiconductor substrates (76 mm quartz substrates). The reason for using microelectronic fabrication is to broaden the available fabrication options. Microelectronic fabrication allows several design of experiments based on various metals, dielectrics and substrates. The fabrication process used to create these structures consisted of evaporating titanium (Ti) adhesion layer and gold (Au) seed layer. A photolithography process was used to define the SRR and the traces. The SRRs and traces were electroplated with gold onto the seed layer to define the final structures. The extra titanium and gold evaporated layers were then removed leaving only the SRRs and traces on the quartz substrate. Figure 2 shows the completed samples made on the FR4 PCB and on the quartz substrates. The FR4 PCB samples have rough edges, resulting from the milling process; while the samples fabricated using the microelectronic techniques have much smaller minimum feature sizes and greater resolution. The rough edges and minimum feature sizes have the effect of reducing the magnitude of the resonant null and location of the resonant frequency.

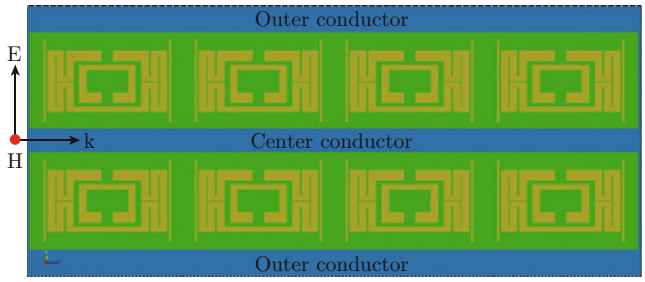

Fig. 3 Meta-atoms inserted in the RF strip-line between the center and outer conductor. The signals propagating down the strip-line generate planar electric and magnetic wave from the center to the outer conductor.

Simulations

Simulations of the three designs are performed in CoventorWare®. This simulation package provides its own unique approach to solve for capacitance and inductance parameters. The CoventorWare® package was used to simulate the designs and determine the capacitance and induction of each design based on FEM and integral equation approach, respectively. The simulations are completed on a single meta-atom using periodic boundary conditions to obtain the design's effective parameters.

The three designs are meshed to perform finite element modeling and boundary element modeling on the 3D designs to obtain the capacitance values. The static designs are simulated in frequency range from 1 MHz to 10 GHz to determine the capacitance and inductance of the design across a broad spectrum. To obtain inductance values, the simulated designs are biased with one volt across the gaps of the inner and outer rings. The one volt bias stimulates a current flow through the rings similar to an induced current on the rings at the SRR capacitive gaps. Figure 4 shows the imaginary current

density of each design simulated with CoventorWare® used to solve for capacitance and inductance. As shown in the Fig. 4, the magnitude of the imaginary current density increases relative to the increase in inductance.

The metal SRR structures are constructed with copper (FR4 PCB prototypes) or gold (microelectronic fabrication) to eliminate any unwanted inductance shifts as a function of the metal or frequency. The range of operation is well below the plasma frequency of copper or gold where metals lose their complex refractive index form and become transparent.

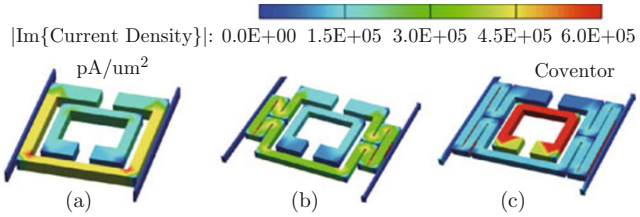

Fig. 4 CoventorWare® plots showing magnitude of imaginary current density incident on the (a) Baseline, (b) Loop A and (c) Loop B versions of the meta-atom designs.

The CoventorWare® simulations show a large inductance change can be achieved with minimal capacitance change. Table 1 lists the inductance and capacitance values obtained from the modeling and simulations. All designs show a shift in the resonance towards a lower frequency.

Table 1 Inductance and capacitance values obtained during modeling and simulations

Design	Baseline	Loop A	Loop B
Outer Ring Inductance (nH)	26.19	31.73	46.94
Inner Ring Inductance (nH)	13.87	13.87	13.87
$C_{Section\_B}$ (pF)	0.04	0.04	0.04
$C_{Section\_C}$ (pF)	0.037	0.037	0.037
C_{Left_Side} (pF)	0.128	0.15	0.153
C_{Right_Side} (pF)	0.128	0.15	0.153
C_{Traces} (pF)	0.053	0.106	0.106
Resonant Frequency (GHz)	2.70	2.33	2.20

Test Results

Two samples of the 1 x 4 array of each SRR meta-atom design (Baseline, Loop A, Loop B) were tested between the inner and outer conductor using an RF strip-line test fixture. The meta-atom arrays are inserted into a 4 GHz strip-line oriented normal to the transverse electromagnetic mode for RF testing (i.e. parallel to the propagation vector). An Agilent Technologies E8362B programmable network analyzer was then used to measure S-parameters within the 1.5-3.5 GHz spectrum incident on the meta-atom arrays.

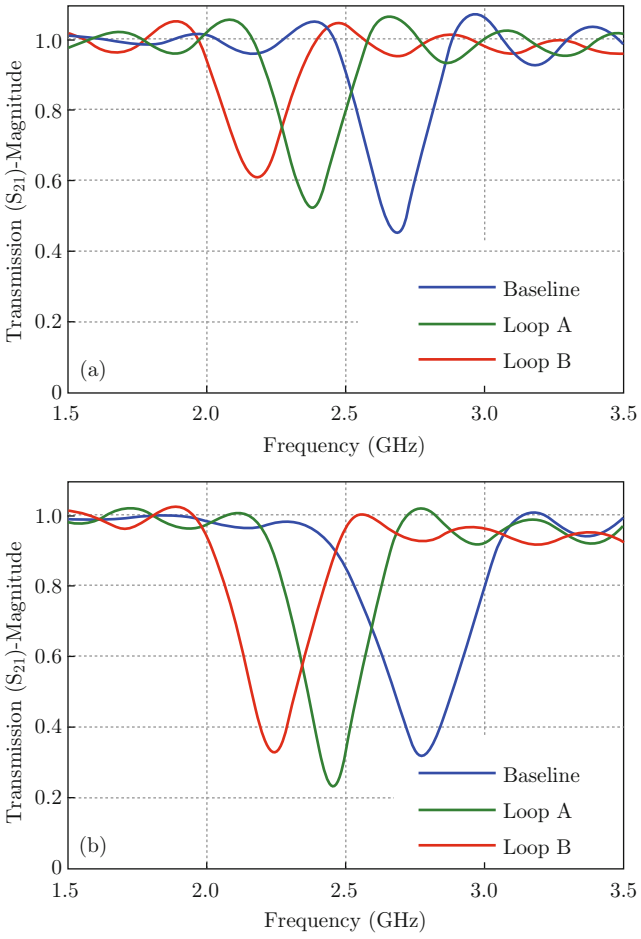

Fig. 5 (a) Data collected on meta-atoms fabricated on FR4 printed circuit board. (b) Data collected on meta-atoms fabricated on quartz substrates. The samples are measured in a 4 GHz strip-line to obtain the small signal S-parameters.

The resonance frequency shifted based on the different designs as expected, matching the simulation results for the Baseline, Loop A, and Loop B designs. The resonant frequency for the Baseline, Loop A and Loop B designs fabricated on printed circuit board (FR4 PCB) are 2.68, 2.37 and 2.18 GHz, respectively. The designs fabricated on quartz wafers showed resonant responses at 2.78, 2.45, and 2.24 GHz, respectively. The difference is attributed to the dielectric constants of the two substrates and the level of resolution for the two fabrication methods. The resonant frequency of each fabrication process design is shown in Fig. 5. The experimental data collection is close to the simulation results shown in Table 1. Figure 5 (a) shows the data collected from two arrays of FR4 PCB meta-atoms spaced

10 mm apart which form a 2D structure. Figure 5 (b) shows the data collected from two arrays of quartz substrate meta-atoms spaced 10 mm apart also forming a 2D structure. Increasing the loop size causes the resonance to shift to a lower frequency with the greatest shift occurring on the Loop B design which the loop equals the vertical side of the outer SRR ring as shown in Fig. 2. Adding more meta-atom arrays and increasing the size of the 2D structure in the RF stripline increases the magnitude of the resonant frequency null.

The simulation and experimental testing results are similar to those published by other authors with comparable meta-atom designs at RF size structures. For example, Pendry *et al.* show results on the circular split-ring resonator at 8.5 GHz [3]. Smith *et al.*, who followed up with Pendry's work on split ring-resonators, experimentally demonstrates the resonant responses at 8.5-9.0 GHz [2] and 4.8 GHz [4]. And as a follow-up to the modeling and simulation based on research conducted by Marques *et al.* we include a comparison to the resonant frequency response described in their papers where they experimentally demonstrate a resonant frequency at 5.45 GHz [8].The main difference is our designs focuses on using inductance as the attributable factor to shift the resonant frequency response for the meta-atoms.

Conclusion

A Baseline SRR design was modified to increase the overall design inductance and minimize capacitance changes. For the FR4 PCB prototype samples, the Loop A, and Loop B designs changed the initial resonant frequency from 2.68 to 2.37 and 2.18 GHz, respectively resulting in a 0.31, and 0.5 GHz change in resonance, respectively. For the quartz samples, the Loop A, and Loop B designs changed the initial resonant frequency from 2.78 to 2.45 and 2.24 GHz, respectively resulting in a 0.33, and 0.53 GHz change in resonance, respectively. Overall, the theory and simulations of the Loop A and Loop B designs matched the experimental results and varying inductance was shown to be a viable method of varying SRR resonance frequencies.

Acknowledgement

The authors would like to thank the AFRL, Sensors Directorate for assistance and advice during device fabrication, Matthew E. Jussaume and Charles McNeely for support during RF testing and Rick Patton and Rich Johnston for AFIT clean room support.

References

[1] J. B. Pendry, A. J. Holden, W. J. Stewart and I. Youngs, Phys. Rev. Lett. 76, 4773 (1996). http://dx.doi.org/10.1103/PhysRevLett.76.4773

[2] D. R. Smith, S. Schultz, P. Markos and C. M. Souloulis, Phys. Rev. B 65, 195104-1 (2002). http://dx.doi.org/10.1103/PhysRevB.65.195104

[3] J. B. Pendry, A. J. Holden, D. J. Robbins and W. J. Stewart, IEEE Trans. Microw. Theory Tech. 47, 2075 (1999). http://dx.doi.org/10.1109/22.798002

[4] D. R. Smith, W. J. Padilla, D. C. Vier, S. C. Nemat-Nasser and S. Schultz, Phys. Rev. Lett. 84, 4184 (2000). http://dx.doi.org/10.1103/PhysRevLett.84.4184

[5] N-H. Shen, M. Kafesaki, T. Koschny, L. Zhang, E. N. Economou and C. M. Soukoulis, Phys. Rev. B 79, 161102-1 (2009). http://dx.doi.org/10.1103/PhysRevB.79.161102

[6] X. Chen, T. M. Grzegorczyk, B-I. Wu, J.Pacheco, Jr. and J. A. Kong, Phys. Rev. E 70, 016608-1 (2004). http://dx.doi.org/10.1103/PhysRevE.70.016608

[7] E. A. Moore, D. Langley, M. E. Jussaume, L. A. Rederus, C. A. Lundell, R. A. Coutu, Jr., P. J. Collins and L. A. Starman, IEEE/ASME J. Microelectro. Systems 20, 1366 (2011).

[8] R. Marqués, J. Martel, F. Mesa and F. Medina, Microw. Opt. Tech. Lett. 35, 405 (2002). http://dx.doi.org/10.1002/mop.10620

[9] V. Zhurbenko, "Passive Microwave Components and Antenna", Rijeka: InTech Publications (2010). http://dx.doi.org/10.5772/226

[10] E. A. Moore, D. Langley, M. E. Jussaume, L. A. Rederus, C. A. Lundell, R. A. Coutu, Jr., P. J. Collins and L. A. Starman, Experimental Mechanics 52, 395 (2011). http://dx.doi.org/10.1007/s11340-011-9498-8

[11] I. Gil, J. Bonache, J. García-García and F. Martín, IEEE Trans. Microw. Theory Tech. 54, 2665 (2006). http://dx.doi.org/10.1109/TMTT.2006.872949

[12] D. Huang, E. Poutrina and D. R. Smith, Appl. Phys. Lett. 96, 104104-1 (2010). http://dx.doi.org/10.1063/1.3356223

[13] J. Zhou, T. Koschny, M. Kafesaki, E. N. Economou, J. B. Pendry and C. M. Soukoulis, Phys. Rev. Lett. 95, 223902-1 (2005). http://dx.doi.org/10.1103/PhysRevLett.95.2239021

[14] 4. M. F. Khan and M. J. Mughal, "Propagation and EMC Technologies for Wireless Communications", IEEE 2009 Int. Symp. Microwave, Antenna, 140 (2009).

[15] P. Jin and R. W. Ziolkowski, IEEE Transactions on Antennas and Propagation 58, 318 (2010). http://dx.doi.org/10.1109/TAP.2010.2078477

[16] R. Marques, F. Medina and R. Rafii-El-Idrissi, Phys. Rev. B 65, 144440-1 (2002). http://dx.doi.org/10.1103/PhysRevB.65.144440$\delimiter"026E30F$

[17] S. A. Ramakrishna and T. M. Grzegorczyk, "Physics and Applications of Negative Refractive Index Materials", SPIE PRESS, Bellingham (2009).

[18] K. Aydin and E. Ozbay, J. Appl. Phys. 101, 024911-1 (2007). http://dx.doi.org/10.1063/1.2427110

[19] 19. A. E. Ruehli, IBM J. Res. Develop. 16, 470 (1972). http://dx.doi.org/10.1147/rd.165.0470

[20] CoventorWare® for MEMS CAD Design, Multiphysics Modeling and Simulation. http://www.coventor.com/coventorware.html